High-pressure synthesis of half-doped perovskites $MnV_{0.5}Nb_{0.5}O_3$ and $MnV_{0.5}Ta_{0.5}O_3$ with unusual A-site small Mn^{2+} cations

Xun Kang,[1,2,*] Hiroaki Hayashi,[1,2], Alexei A. Belik,[1] Yoshihiro Tsujimoto,[1,2] and Kazunari Yamaura [1,2]

[1] Research Center for Materials Nanoarchitectonics (MANA), National Institute for Materials Science, 1-1 Namiki, Tsukuba, Ibaraki 305-0044, Japan
[2] Graduate School of Chemical Sciences and Engineering, Hokkaido University, North 10 West 8, Kita-ku, Sapporo, Hokkaido 060-0810, Japan

Abstract

We have successfully synthesized two new half-doped perovskites, $MnV_{0.5}Nb_{0.5}O_3$ and $MnV_{0.5}Ta_{0.5}O_3$, with unique small Mn^{2+} cations at the A site under high-temperature and high-pressure conditions (6 GPa and 900-1300 °C). Synchrotron X-ray structure analysis confirmed their crystal structures to belong to the space group *Pnma*, and they do not exhibit features of an ordered perovskite (double perovskite) structure. Magnetic property measurements revealed an essentially antiferromagnetic nature below 17 K and 18 K for both compounds, respectively, accompanied by a small contribution of thermal and magnetic field hysteresis. Electrical conductivity measurements showed activation energies of 0.13 eV and 0.31 eV, respectively, suggesting semiconductor-like behavior. These findings underscore the potential of these materials with unusual A-site small Mn^{2+} cations for electronic and magnetic devices, warranting further studies to explore their unique magnetic and electronic properties.

Keywords

Perovskites, $MnVO_3$, $MnV_{0.5}Nb_{0.5}O_3$, $MnV_{0.5}Ta_{0.5}O_3$, Synchrotron XRD, High-pressure synthesis

[*] **To whom corresponding should be addressed.**
Quantum Solid State Materials Group
Research Center for Materials Nanoarchitectonics (MANA)
National Institute for Materials Science
1-1 Namiki, Tsukuba, Ibaraki 305-0044, Japan
E-mail: KANG.Xun@nims.go.jp

1. Introduction

Perovskites have been a prominent research area for several decades and have garnered significant attention due to the intriguing phenomena exhibited by ABO_3-type perovskite oxides. These phenomena include ferroelectricity in materials like $BaTiO_3$ [1–3], $SrTiO_3$ [4,5], $PbTiO_3$ [6,7], $KNbO_3$ [8,9], high-T_c superconductivity in $BaPb_{1-x}Bi_xO_3$ [10], colossal magnetoresistance in $NdBaMn_2O_6$ [11], $LaMnO_3$ [12], Sr_2CrWO_6 [13], charge/orbital ordering in $Ln_{1-x}A_xMnO_3$ (Ln = rare earth element, A = Ca, Sr) [14], $Sm_{0.5}Ba_{0.5}MnO_3$ [15], $PbFeO_3$ [16], multiferroicity in $BiCrO_3$ [17], $BiMnO_3$ [18,19], and $BiFeO_3$ [20,21], superconductivity in (Ba, K)SbO_3 [22], $MgCNi_3$ [23], photoelectricity in $CsPbX_3$ (X = Br, I) [24], exotic magnetism in Ca_2MnReO_6 [25], and significant thermoelectricity in $CsSnI_3$ [26], among others. These properties make them highly promising materials for both scientific investigations and industrial applications.

Usually, transition-metal cations occupy B-sites, while larger alkaline-earth or rare-earth elements locate in A-sites. In 1971, Shono *et al*. [27] demonstrated that under high-pressure conditions, it is possible to fill the A-sites with relatively small transition metal cations, leading to the synthesis of perovskite-type $MnVO_3$. Introducing magnetic elements at A-sites can induce exotic properties, such as ferroelectricity or magnetic ferroelectricity, through strong interactions with elements at B-sites. Consequently, extensive research into unusual A-site manganese was undertaken to explore their unique magnetic and electronic properties, leading to the discovery of many excellent properties, such as multiferroism in $CaMnTi_2O_6$ [28] and the unusual site-selective doping effect in $AMn_3V_4O_{12}$ (A = Na^+, Ca^{2+}, La^{3+}) [29]. Notably, in 2015, Arévalo *et al*. reported a double perovskite Mn_2FeReO_6 [30], which exhibits a high Curie temperature of 520 K and displays large magnetoresistance, making it a significant candidate for potential applications in spintronics. Subsequently, canted antiferromagnetic properties were identified in Mn_2MnReO_6 [31], unconventional magnetism in Mn_2NiReO_6 [32], and multiple transition metal sublattice magnetic effects in $Mn_2(Fe_{0.8}Mo_{0.2})MoO_6$ [33], providing further insights into the rich magnetic behavior of these materials.

Therefore, the search for unusual A-site manganese oxides with unique magnetic and electronic properties holds great potential for the scientific design, theoretical exploration, and practical application of new materials. In this study, we explored the properties of $MnVO_3$, first synthesized in 1971 [27], and introduced d^0 ions, Nb^{5+} and Ta^{5+}, into the structure to explore possible magnetic ferroelectricity. Consequently, $MnV_{0.5}Nb_{0.5}O_3$ was synthesized under high-pressure and high-temperature conditions of 6 GPa and 1300°C, respectively, while $MnV_{0.5}Ta_{0.5}O_3$ was synthesized at 6 GPa and 900°C. Structural analysis by synchrotron radiation X-ray diffraction confirmed that both $MnV_{0.5}Nb_{0.5}O_3$ and $MnV_{0.5}Ta_{0.5}O_3$ are half-doped perovskite oxides and not double perovskite oxides. Furthermore, the absence of a polar structure indicated that the materials do not exhibit ferroelectricity at room temperature. However, magnetization measurements confirmed antiferromagnetic ordering at 17 K and 18 K for $MnV_{0.5}Nb_{0.5}O_3$ and $MnV_{0.5}Ta_{0.5}O_3$, respectively, with a slight contribution of thermal and magnetic field hysteresis. Additionally, both compounds also exhibit semiconducting behavior at estimated activation energies of about 0.13 eV and 0.31 eV, respectively. Unfortunately, the observed electrical conductivity in these materials posed challenges in performing accurate dielectric measurements, as it could introduce significant noise in the data, hindering the assessment of their response to electric fields and their potential as ferroelectrics. The observed antiferromagnetic nature and semiconducting behavior in these A-site

manganese oxides underscore the potential of these materials for future research in the exploration of their unique magnetic and electronic properties.

2. Experimental

Polycrystalline $MnV_{0.5}Nb_{0.5}O_3$ and $MnV_{0.5}Ta_{0.5}O_3$ were synthesized using high-purity materials: MnO (99.99%, High Purity Chemical Co. Ltd.), V_2O_3 (99.99%, High Purity Chemical Co. Ltd.), Nb_2O_5 (99.9%, Rare Metallic Co. Ltd.), and Ta_2O_5 (99.9%, Rare Metallic Co. Ltd.). The powders of MnO, V_2O_3, and Nb_2O_5 (or Ta_2O_5) were mixed in stoichiometric ratios and then pressed into pellets after thorough grinding. Subsequently, the $MnV_{0.5}Nb_{0.5}O_3$ sample was enclosed in a Pt capsule. This capsule was then placed within a high-pressure cubic setup using a multi-anvil-type high-pressure apparatus (CTF-MA1500P, C&T Factory Co., Ltd, Japan), with a layer of graphite enveloping the capsule. By applying an electric current, the graphite layer generated significant heat, heating the enclosed capsule at 1300 °C for 1 hour under a pressure of 6 GPa. Following the heating process, the pressure was gradually released over several hours. The synthesis procedure for $MnV_{0.5}Nb_{0.5}O_3$ was similar, but the temperature used was 900 °C.

Synchrotron X-ray diffraction (XRD) data were collected at room temperature using a large Debye-Scherrer camera at beamline BL02B2 at SPring-8, Japan [34,35]. The incident beam was monochromatized at a wavelength of λ = 0.420259 Å. To ensure accurate measurements, a benchmark test was conducted using a standard material (CeO_2) to confirm the wavelength. The samples were loaded into Lindemann glass capillaries with an inner diameter of 0.1 mm and rotated during the measurements. The synchrotron XRD patterns were analyzed using the RIETAN-VENUS software package [36,37].

Magnetic properties were investigated using a magnetic property measurement system (MPMS-XL-7T, Quantum Design). Magnetic susceptibilities (χ) were measured over the temperature range of 2 to 300 K, under both zero-field-cooling (ZFC) and field-cooling (FC) conditions, in a fixed applied magnetic field of 10 kOe. Isothermal magnetization measurements were conducted at temperatures of 5 K and 50 K, spanning magnetic fields between 70 kOe and -70 kOe.

The electrical properties and specific heat of both $MnV_{0.5}Nb_{0.5}O_3$ and $MnV_{0.5}Ta_{0.5}O_3$ were measured using a Physical Property Measurement System (PPMS, Quantum Design). The temperature dependence of electric resistivity (ρ) was recorded using a four-probe method, with the temperature range for $MnV_{0.5}Nb_{0.5}O_3$ being approximately 140-300 K. To establish connections between the sample and the device terminals, silver paste and platinum wires (50 μm in diameter) were utilized. The measured current during the experiments was maintained at 1 mA. Furthermore, the temperature dependence of specific heat capacities (C_p) was measured using the same machine, employing a thermal relaxation method. These measurements were conducted over the temperature range from 2 to 300 K.

3. Results and discussion

Crystal Structure: The analyzed synchrotron XRD patterns and the refined crystallographic parameters of both $MnV_{0.5}Nb_{0.5}O_3$ and $MnV_{0.5}Ta_{0.5}O_3$ obtained at room temperature are presented in Fig. 1 and Table 1, respectively. In the Rietveld refinement, the crystal structure model proposed for $MnVO_3$ was employed as the prototype. Both compounds were successfully identified with the

space group *Pnma*. A trace impurity of $MnNb_2O_6$ (5.3 wt.%) was detected in $MnV_{0.5}Nb_{0.5}O_3$, while a $VTaO_4$ (2.5 wt.%) impurity was observed in $MnV_{0.5}Ta_{0.5}O_3$.

The lattice constants of $MnV_{0.5}Nb_{0.5}O_3$ were calculated as follows: a = 5.40739(7) Å, b = 7.59492(9) Å, c = 5.22262(6) Å. Similarly, for $MnV_{0.5}Ta_{0.5}O_3$, the lattice constants were determined as: a = 5.41934(3) Å, b = 7.61121(4) Å, c = 5.23227(2) Å. While exploring possible double perovskite structure models reported for other Mn-containing compounds at the A-site of double perovskite oxides [30–32], we found them to be unlikely to fit the observed patterns due to the absence of a series of superstructure diffraction peaks caused by ordered B-site atoms.

Analysis of the refinement results reveals that Mn atoms fully occupy the 4*c* (x, 0.25, z) Wyckoff positions, while V and Nb/Ta atoms are randomly distributed in the 4*a* (0, 0, 0) sites. Although there are some impurities present in the sample, their content is minimal. Due to the limitations of the experimental conditions, more precise compositional measurements were not feasible. Therefore, the ratio of V and Nb/Ta was fixed at 1:1 in the refinements, based on the stoichiometry of the starting raw materials. Oxygen atoms O1 and O2 are located at independent positions, 4*c* (x, 0.25, z) and 8*d* (x, y, z), respectively. The final detailed lattice parameters, atomic coordinates, and temperature factors are summarized and presented in Table 1.

Table 1: Structure Parameters of $MnV_{0.5}Nb_{0.5}O_3$ and $MnV_{0.5}Ta_{0.5}O_3$.

Atom	Wyckoff	*g*	*x*	*y*	*z*	*B* (Å^2)
			$MnV_{0.5}Nb_{0.5}O_3$			
Mn	4*c*	1	0.0515(3)	0.25	0.4875(5)	1.23(5)
V/Nb	4*a*	0.5/0.5	0	0	0	0.61(2)
O1	4*c*	1	0.4558(13)	0.25	0.6092(11)	0.12(16)
O2	8*d*	1	0.2994(10)	0.0591(6)	0.1892(9)	0.65(1)
			$MnV_{0.5}Ta_{0.5}O_3$			
Mn	4*c*	1	0.0510(2)	0.25	0.4878(5)	1.48(3)
V/Ta	4*a*	0.5/0.5	0	0	0	0.58(1)
O1	4*c*	1	0.4561(11)	0.25	0.6164(10)	0.40(12)
O2	8*d*	1	0.3032(8)	0.0588(5)	0.1899(8)	0.65(9)

Note. The space group was *Pnma* (no. 62) at origin choice 2, Z = 4, and g was the occupation factor. $MnV_{0.5}Nb_{0.}5O_3$: a = 5.40739(7) Å, b = 7.59492(9) Å, c = 5.22262(6) Å and V = 412.669(10) Å^3. R Indices are R_{wp} = 5.343%, R_p = 3.859%, R_B = 6.608%, and R_F = 7.208%. $MnV_{0.5}Ta_{0.5}O_3$: a = 5.41934(3) Å, b = 7.61121(4) Å, c = 5.23227(2) Å and V = 412.669(10) Å^3. R Indices are R_{wp} = 8.232%, R_p = 4.724%, R_B = 5.532%, and R_F = 4.151%.

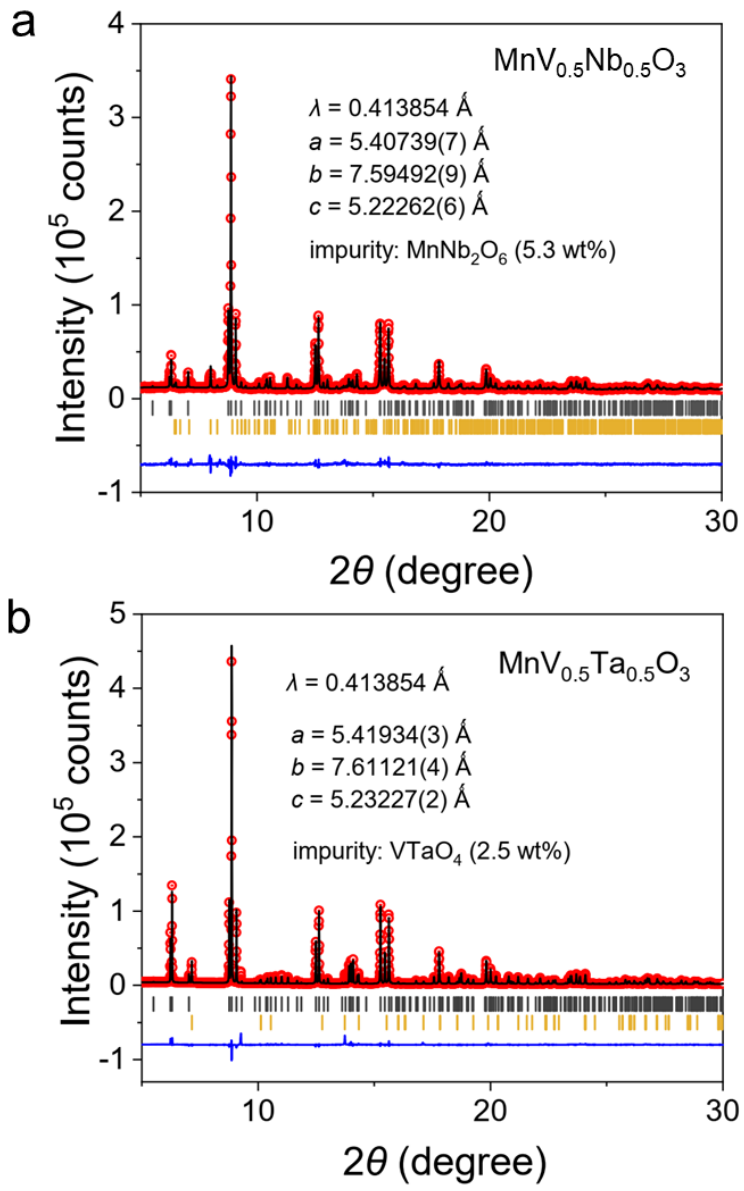

Figure 1: Synchrotron XRD data for $MnV_{0.5}Nb_{0.5}O_3$ and $MnV_{0.5}Ta_{0.5}O_3$ in the orthorhombic *Pnma* structure at room temperature (296-300 K). Each panel displays the observed pattern (red circles), calculated pattern (black solid lines), and the difference profile (blue curves). Vertical bars indicate possible Bragg reflection positions for the main phase (the first row) and the impurity (the second row).

For clarity, we selected one compound for illustration (Fig. 2a), as both compounds crystallize in the same *Pnma* space group. The left side of the figure shows the crystal structure observed along the c-axis, with a slight shift in the direction of observation for enhanced visibility. On the right side is the view perpendicular to the c-axis. Notably, both compounds exhibit octahedral distortions and connected twisting compared to the ideal cubic perovskites.

In Fig. 2b, a comparison of the lattice parameters and unit cell volumes of $MnV_{0.5}Nb_{0.5}O_3$ and $MnV_{0.5}Ta_{0.5}O_3$ with the related compound $MnVO_3$ is present. Here, the horizontal coordinates are labelled with elements rather than ionic radii, as Nb^{5+} and Ta^{5+} share the same ionic radii. Thus,

we provide a listing of 3d, 4d, and 5d elements. The comparison clearly indicates that the lattice parameters and unit cell volumes increase monotonically with the increase of atomic numbers.

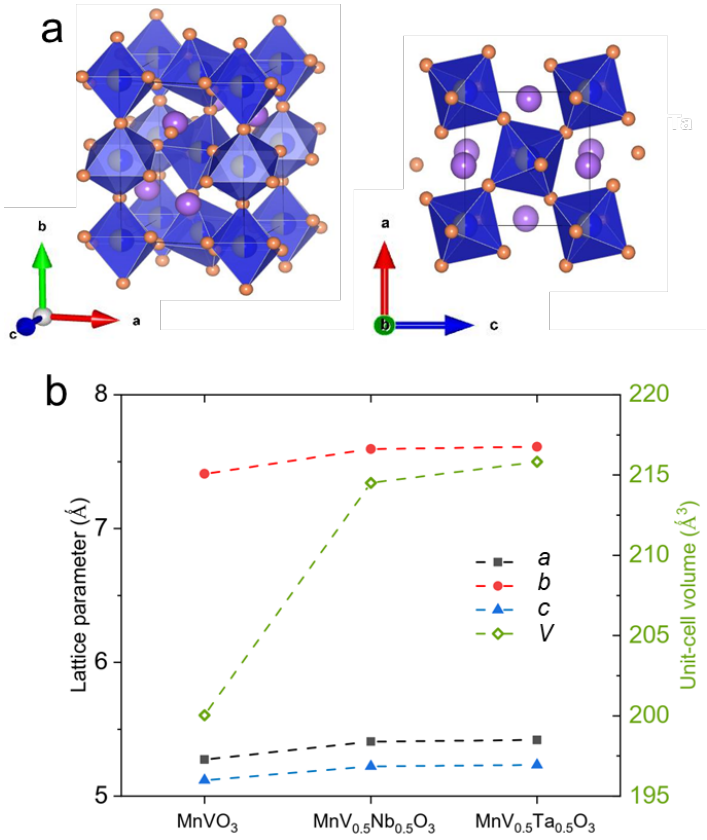

Figure 2: (a) Crystal structure for $MnV_{0.5}Nb_{0.5}O_3$ and (b) a comparison of lattice parameters with $MnV_{0.5}Ta_{0.5}O_3$ and $MnVO_3$.

The valence states of Mn, V, and Nb (or Ta) atoms were determined based on the bond distances in different compounds, and the bond valence sums (BVS) [38] results are presented in Table 2. The BVS calculations for Mn in both $MnV_{0.5}Nb_{0.5}O_3$ and $MnV_{0.5}Ta_{0.5}O_3$ yielded a value of 1.82, indicating a 2+ valence state for Mn in both compounds. The BVS values for the V atoms corresponded to 3+, and for Nb (or Ta) atoms, they were very close to 5+, suggesting the effectiveness of the BVS method for determining the valence states of these elements in the compounds.

Table 2: Selected bond lengths, angles, and BVS of $MnV_{0.5}Nb_{0.5}O_3$ and $MnV_{0.5}Ta_{0.5}O_3$ at room temperature (296-300 K).

$MnV_{0.5}Nb_{0.5}O_3$	Bond lengths (Å); BVS; bond angles (º)	$MnV_{0.5}Ta_{0.5}O_3$	Bond lengths (Å); BVS; bond angles (º)
Mn – O1	3.159(7)	Mn – O1	3.203(6)
Mn – O1	3.283(8)	Mn – O1	4.273(3)
Mn – O1	2.277(8)	Mn – O1	2.296(6)
Mn – O1	2.169(7)	Mn – O1	2.134(6)
Mn – O2 (×2)	2.515(6)	Mn – O2 (×2)	2.695(5)

Mn – O2 (×2)	2.194(6)	Mn – O2 (×2)	2.188(5)
Mn – O2 (×2)	2.697(6)	Mn – O2 (×2)	2.533(5)
Mn – O2 (×2)	3.459(6)	Mn – O2 (×2)	3.471(5)
BVS (Mn)	1.82	BVS (Mn)	1.82
V/Nb – O1 (×2)	1.997(2)	V/Ta - O1 (×2)	2.012(2)
V/Nb – O2 (×2)	1.949(6)	V/Ta – O2 (×2)	1.971(5)
V/Nb – O2 (×2)	2.003(6)	V/Ta – O2 (×2)	1.993(5)
BVS (V)	3.14	BVS (V)	3.06
BVS (Nb)	4.95	BVS (Ta)	4.94
V(Nb) – O1 – V(Nb)	143.9(4)	V – O1 – V	142.1(3)
V(Nb) – O2 – V(Nb)	144.0(3)	V – O2 – V	143.7(3)

Note. BVS = $\sum_{i=1}^{N} v_i$, $v_i = \exp[(R_0 - l_i)/B]$, N is the coordination number, B = 0.37, $R_0(Mn^{2+}) = 1.79$, $R_0(V^{3+}) = 1.743$, $R_0(Nb^{5+}) = 1.911$, $R_0(Ta^{5+}) = 1.920$ [38].

Magnetic property: The temperature dependence of χ under an applied magnetic field of 10 kOe for both compounds is shown in Fig. 3. Peaks were observed at around 17 K and 18 K for $MnV_{0.5}Nb_{0.5}O_3$ and $MnV_{0.5}Ta_{0.5}O_3$, respectively. The χ^{-1} vs. T data (200 - 300 K) were fitted using the Curie-Weiss law (see the inset of Fig. 3), resulting in Curie constants of 3.94 and 4.92 emu mol^{-1} K^{-1} (equivalent to effective magnetic moments of 5.61 and 6.27 μ_B), and Weiss temperatures of -95.9 K and -92.56 K for $MnV_{0.5}Nb_{0.5}O_3$ and $MnV_{0.5}Ta_{0.5}O_3$, respectively. Theoretical calculations within the simple spin-only model predicted a magnetic moment of 6.25 μ_B for all compounds. Remarkably, the observed effective magnetic moments were comparable to the theoretical results. The large negative Weiss temperatures indicate the presence of antiferromagnetic interactions in these compounds.

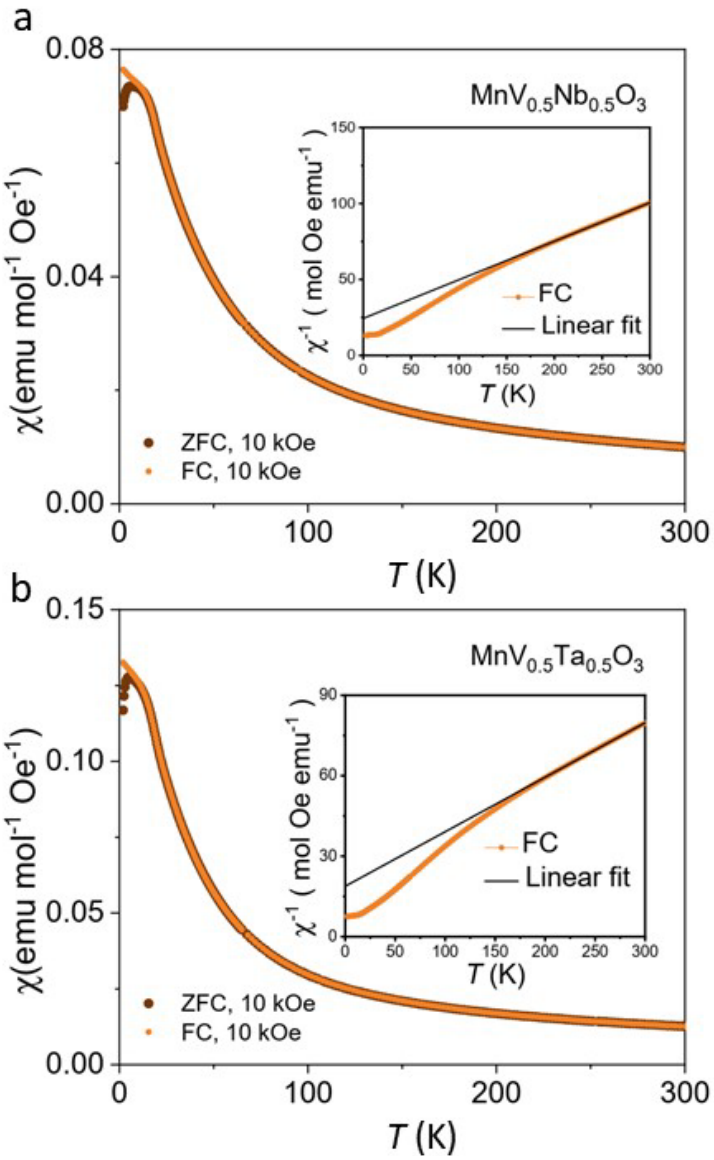

Figure 3: (a) Temperature dependence of magnetic susceptibility (χ) for $MnV_{0.5}Nb_{0.5}O_3$ and (b) $MnV_{0.5}Ta_{0.5}O_3$. Insets show the χ^{-1} vs. T curves used for the Curie-Weiss law fittings.

From the ZFC and FC curves, we observe divergence at low temperatures, suggesting that the compounds may exhibit antiferromagnetic or spin-glass behavior at low temperatures. To investigate the intrinsic nature of the magnetic ground state, we plotted the isothermal magnetization curves at 5 K and 50 K in Fig. 4. Even at 5 K and below 7 T, the magnetizations do not saturate, and the values are approximately 0.8 μ_B per formula unit (f.u.) for $MnV_{0.5}Nb_{0.5}O_3$ and 1.0 μ_B per f.u. for $MnV_{0.5}Ta_{0.5}O_3$, far below the expected spin-only value of 6 μ_B per f.u. The linear $M(H)$ curves at 50 K suggest the paramagnetic states, while the typical 'S'-shaped hysteresis loops at 5 K indicate the presence of either antiferromagnetic ordering or spin-glass behavior in the samples. To precisely determine the spin alignments, we conducted heat capacity measurements to confirm the accurate magnetic behavior of the samples.

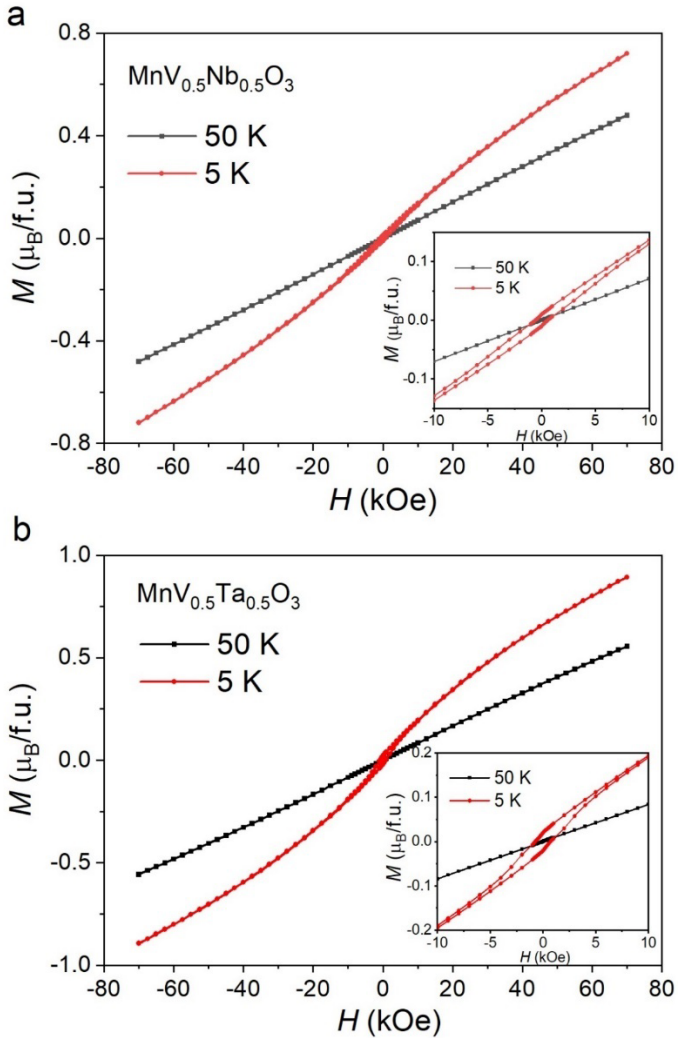

Figure 4: (a) Magnetic field-dependent magnetization for $MnV_{0.5}Nb_{0.5}O_3$ and (b) $MnV_{0.5}Ta_{0.5}O_3$ at temperatures of 5 and 50 K.

Heat Capacity: To investigate the magnetic transitions, we conducted temperature-dependent C_p measurements for both compounds. The C_p/T vs. T data were recorded during cooling from 300 to 2 K, and the results are presented in Fig. 5. Clear peaks were observed at the magnetic transition temperature points, indicating the presence of long-range order transitions in the compounds. These prominent peaks are likely connected to the splitting observed in the ZFC and FC curves, primarily arising from the long-range antiferromagnetic transition. However, it is worth noting that a magnetic glassy transition cannot be completely ruled out, as evidenced by a peak-like feature in some cases, although a broad hump is typically observed [39]. Further detailed studies will be required to fully elucidate the nature of the magnetic transitions in these compounds.

In the low-temperature region, C_p/T vs. T^2 plots for each compound were analyzed using the approximate Debye model $C_p/T = \beta T^2+\gamma$, where γ is the electronic specific heat coefficient and β is a constant encompassing the Debye temperature Θ_D ($\sim\beta^{1/3}$). For $MnV_{0.5}Nb_{0.5}O_3$, the linear fitting yields $\gamma = 94.0(2)$ mJ mol^{-1} K^{-2} and $\beta = 7.31(2) \times 10^{-3}$ J mol^{-1} K^{-4}, and for $MnV_{0.5}Ta_{0.5}O_3$, $\gamma = 111(1)$ mJ mol^{-1} K^{-2} and $\beta = 7.2(1) \times 10^{-3}$ J mol^{-1} K^{-4}. The non-zero γ value usually suggests a significant contribution from conduction electrons to C_p. However, given the compound's lack of electrical

conductivity at low temperatures, an alternative origin for γ is likely, possibly related to magnetic ordering or other magnetic effects. Further comprehensive investigation is needed to fully elucidate this phenomenon, including a study of the magnetic field dependence of C_p, additional density functional theory (DFT) calculations, and a detailed analysis of the magnetic properties of the compounds. These approaches will offer valuable insights into the specific heat behavior of $MnV_{0.5}Nb_{0.5}O_3$ and $MnV_{0.5}Ta_{0.5}O_3$ at low temperatures and the underlying mechanisms.

Furthermore, we delved deeper into magnetic entropy (S_{mag}) to gain a more profound understanding of the magnetic properties. The magnetic contribution (C_{mag}) was determined by subtracting the lattice contribution ($C_{Lattice}$) from C_p using the Debye and Einstein model [40]. S_{mag} values were estimated by integrating C_{mag}/T. The saturation S_{mag} values for Nb- and Ta-oxides were approximately 12 J mol^{-1} K^{-1} and 14 J mol^{-1} K^{-1}, respectively. Both were lower than the theoretically expected Boltzmann entropy value $S_{mag} = R\ln(2S + 1) = 19.47$ J mol^{-1} K^{-1} [40]. This discrepancy arises from the estimation of the lattice contribution at low temperatures based on high-temperature data using the Debye and Einstein model, which may not accurately reflect the lattice contribution at lower temperatures. Nonetheless, the observed S_{mag} values suggest the potential existence of magnetic entropy even at significantly lower temperatures.

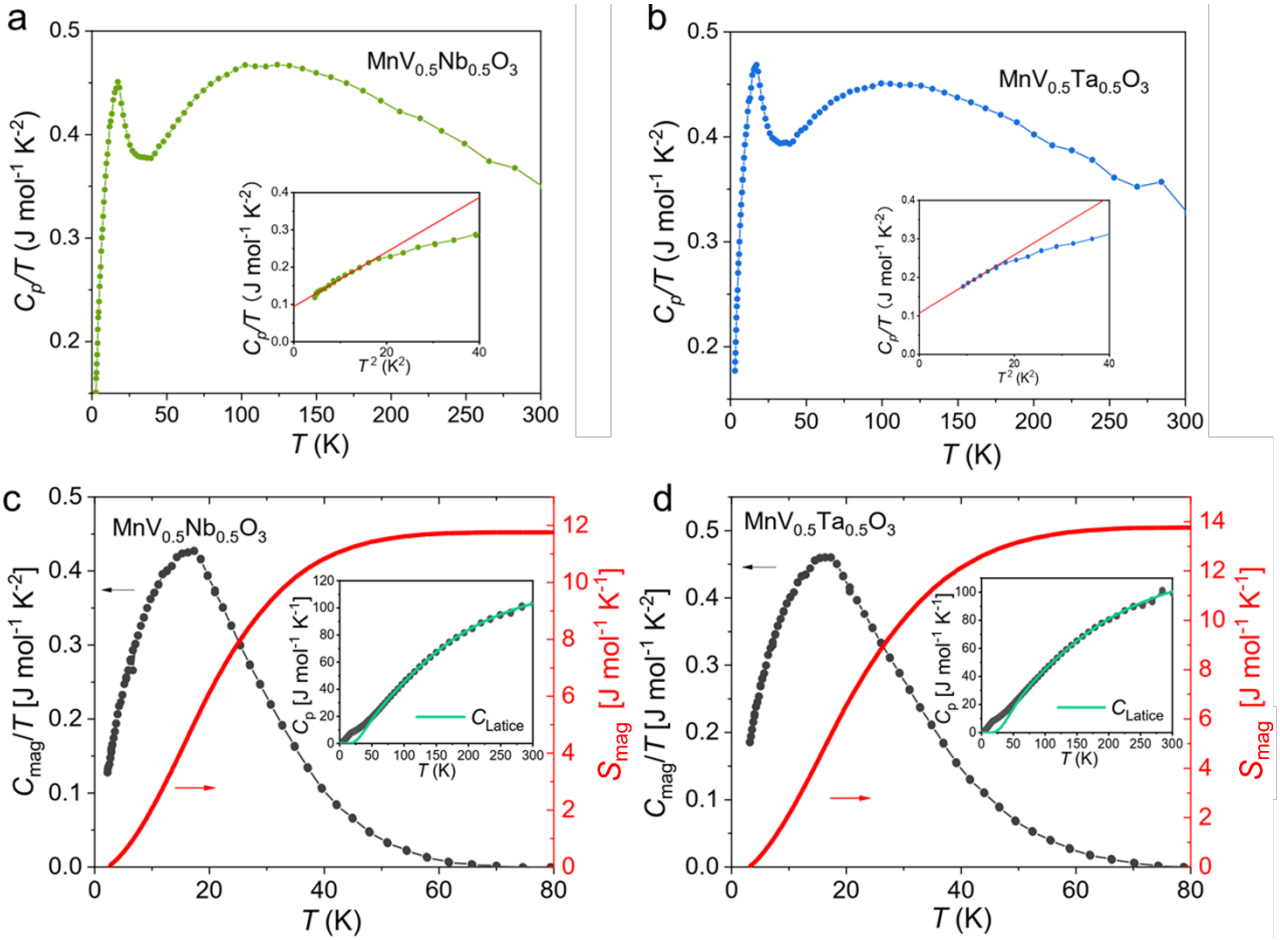

Figure 5: Temperature dependence of C_p for (a) $MnV_{0.5}Nb_{0.5}O_3$ and (b) $MnV_{0.5}Ta_{0.5}O_3$. (Inset) The C_p/T vs. T^2 data in the low-temperature region were fitted using a linear model. Temperature dependences of C_{mag} and S_{mag} for (c) $MnV_{0.5}Nb_{0.5}O_3$ and (d) $MnV_{0.5}Ta_{0.5}O_3$; insets represent C_p and $C_{Lattice}$ obtained by fitting to the high-temperature region with Debye and Einstein models.

Electronic property: The temperature dependence of the ρ for polycrystalline $MnV_{0.5}Nb_{0.5}O_3$ and $MnV_{0.5}Ta_{0.5}O_3$ displayed insulating behaviors, as shown in Fig. 6. The ρ at room temperature were approximately 100 Ω cm and 1000 Ω cm for $MnV_{0.5}Nb_{0.5}O_3$ and $MnV_{0.5}Ta_{0.5}O_3$, respectively, consistent with their semiconductor nature. As the measurement temperature decreased below 130 K for $MnV_{0.5}Nb_{0.5}O_3$ and 200 K for $MnV_{0.5}Ta_{0.5}O_3$, the ρ exceeded the test range of the instrument, making it challenging to obtain measurements at even lower temperatures. Notably, the prototype compound from which they are derived, $MnVO_3$, exhibits metallic properties. The large difference in electrical conductivity observed in $MnV_{0.5}Nb_{0.5}O_3$ and $MnV_{0.5}Ta_{0.5}O_3$ may be attributed to the addition of Nb^{5+} and Ta^{5+} ions, which reduces the valence of V from a 4+ state to a 3+ state. This change causes the absence of itinerant electrons present in the original system and their replacement with pairs of electrons, resulting in a dramatic increase in ρ.

The data were fitted using the Arrhenius equation, and the relative activation energy of $MnV_{0.5}Nb_{0.5}O_3$ and $MnV_{0.5}Ta_{0.5}O_3$ were estimated to be 0.13 eV and 0.31 eV, respectively. These experimentally evaluated values confirm that both compounds exhibit semiconducting behavior. Additionally, we employed the Efros-Shklovskii variable-range hopping conduction model, $\rho = \rho_0 \exp[(T_0/T)^{1/2}]$ [41], to analyze the data, and it was found that the data seem to fit the model well. Further in-depth discussions about the transport properties will be expected after single crystal growth is achieved, and transport measurements are conducted.

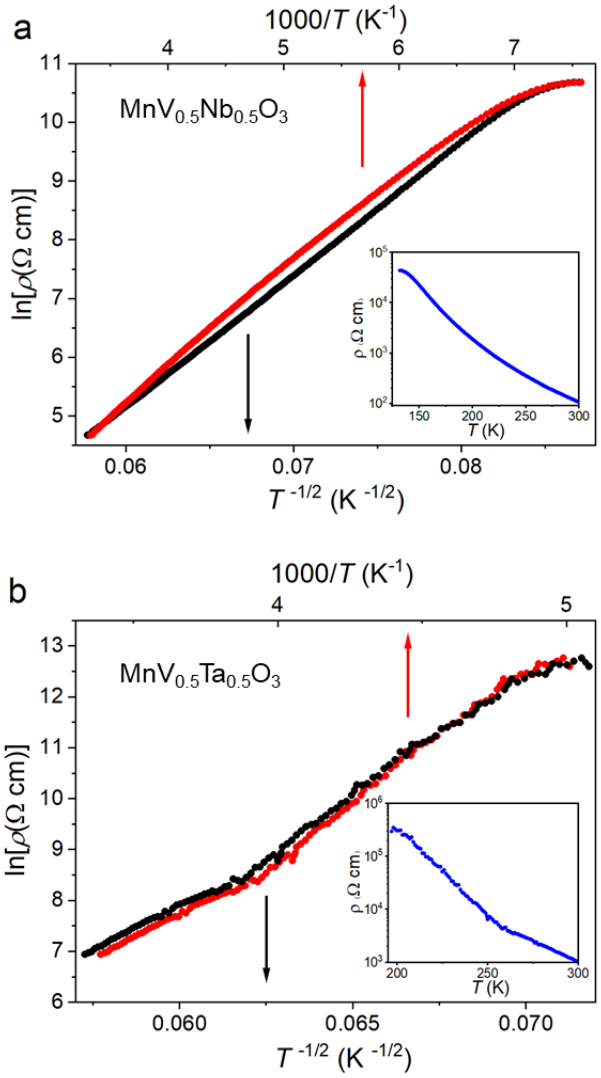

Figure 6: (a) Electrical resistivity (ρ) for $MnV_{0.5}Nb_{0.5}O_3$ and (b) $MnV_{0.5}Ta_{0.5}O_3$.

4. Conclusion

In summary, our study successfully synthesized two novel half-doped perovskites, $MnV_{0.5}Nb_{0.5}O_3$ and $MnV_{0.5}Ta_{0.5}O_3$, with unique magnetic and electronic properties due to the incorporation of small Mn atoms at the A site. The crystallographic analysis confirmed their *Pnma* structure, distinct from an ordered perovskite. Magnetic measurements revealed antiferromagnetic behavior below 17 K and 18 K for the respective compounds, with a slight contribution of hysteresis. Furthermore, the observed semiconductor-like behavior in electrical conductivity highlights their potential for electronic applications. These results underscore the significance of these materials with unusual A-site small Mn atoms and open new avenues for further research into their unique magnetic and electronic properties. Future studies should explore single crystal growth and in-depth transport measurements to advance our understanding and unlock their practical applications in electronic and magnetic devices.

ACKNOWLEDGMENTS

MANA is supported by the World Premier International Research Center Initiative (WPI) of MEXT, Japan. This work was partially supported by a Grant-in-Aid for Scientific Research (No. JP20H05276 and JP22H04601) from the Japan Society for the Promotion of Science and the Kazuchika Okura Memorial Foundation (No. 2022-11). Synchrotron radiation was used at the powder diffraction beamline BL02B2 at SPring-8, with permission from the Japan Synchrotron Radiation Research Institute (Proposal Numbers: 2021A1169, 2022A1067, and 2023A2361).

REFERENCES

[1] Michel VF, Esswein T, Spaldin NA. Interplay between ferroelectricity and metallicity in BaTiO3. J Mater Chem C Mater. 2021;9:8640–8649.
[2] Smith MB, Page K, Siegrist T, et al. Crystal Structure and the Paraelectric-to-Ferroelectric Phase Transition of Nanoscale BaTiO3. J Am Chem Soc. 2008;130:6955–6963.
[3] Cohen RE. Origin of ferroelectricity in perovskite oxides. Nature. 1992;358:136–138.
[4] Xu R, Huang J, Barnard ES, et al. Strain-induced room-temperature ferroelectricity in SrTiO3 membranes. Nat Commun. 2020;11:3141.
[5] Haeni JH, Irvin P, Chang W, et al. Room-temperature ferroelectricity in strained SrTiO3. Nature. 2004;430:758–761.
[6] Bhide VG, Deshmukh KG, Hegde MS. Ferroelectric properties of PbTiO3. Physica. 1962;28:871–876.
[7] Zhang S, Li F. High performance ferroelectric relaxor-PbTiO3 single crystals: Status and perspective. J Appl Phys. 2012;111.
[8] Liang L, Li YL, Chen L-Q, et al. Thermodynamics and ferroelectric properties of KNbO3. J Appl Phys. 2009;106.
[9] Masuda I, Kakimoto K-I, Ohsato H. Ferroelectric Property and Crystal Structure of KNbO3 Based Ceramics. J Electroceram. 2004;13:555–559.
[10] Sleight AW, Gillson JL, Bierstedt PE. High-temperature superconductivity in the BaPb1-xBixO3 systems. Solid State Commun. 1975;17:27–28.
[11] Yamada S, Abe N, Sagayama H, et al. Room-Temperature Low-Field Colossal Magnetoresistance in Double-Perovskite Manganite. Phys Rev Lett. 2019;123:126602.
[12] Baldini M, Muramatsu T, Sherafati M, et al. Origin of colossal magnetoresistance in LaMnO3 manganite. Proceedings of the National Academy of Sciences. 2015;112:10869–10872.
[13] Zhang J, Ji W-J, Xu J, et al. Giant positive magnetoresistance in half-metallic double-perovskite Sr2CrWO6 thin films. Sci Adv. 2017;3.
[14] Rao CNR. Charge, Spin, and Orbital Ordering in the Perovskite Manganates, Ln1-xAxMnO3 (Ln = Rare Earth, A = Ca or Sr). J Phys Chem B. 2000;104:5877–5889.
[15] Uchida M, Akahoshi D, Kumai R, et al. Charge/Orbital Ordering Structure in Ordered Perovskite Sm1/2Ba1/2MnO3. J Physical Soc Japan. 2002;71:2605–2608.
[16] Ye X, Zhao J, Das H, et al. Observation of novel charge ordering and spin reorientation in perovskite oxide PbFeO3. Nat Commun. 2021;12:1917.
[17] Cardoso JP, Delmonte D, Gilioli E, et al. Phase Transitions in the Metastable Perovskite Multiferroics BiCrO3 and BiCr0.9Sc0.1O3 : A Comparative Study. Inorg Chem. 2020;59:8727–8735.
[18] Zhai L-J, Wang H-Y. The magnetic and multiferroic properties in BiMnO3. J Magn Magn Mater. 2017;426:188–194.
[19] Sugawara F, Iiida S, Syono Y, et al. Magnetic Properties and Crystal Distortions of BiMnO3 and BiCrO3. J Physical Soc Japan. 1968;25:1553–1558.
[20] Jia D-C, Xu J-H, Ke H, et al. Structure and multiferroic properties of BiFeO3 powders. J Eur Ceram Soc. 2009;29:3099–3103.

[21] Carranza-Celis D, Cardona-Rodríguez A, Narváez J, et al. Control of Multiferroic properties in BiFeO3 nanoparticles. Sci Rep. 2019;9:3182.
[22] Kim M, McNally GM, Kim H-H, et al. Superconductivity in (Ba,K)SbO3. Nat Mater. 2022;21:627–633.
[23] He T, Huang Q, Ramirez AP, et al. Superconductivity in the non-oxide perovskite MgCNi3. Nature. 2001;411:54–56.
[24] Liu F, Sidhik S, Hoffbauer MA, et al. Highly efficient photoelectric effect in halide perovskites for regenerative electron sources. Nat Commun. 2021;12:673.
[25] Cavichini AS, Orlando MT, Depianti JB, et al. Exotic magnetism and spin-orbit-assisted Mott insulating state in a 3d-5d double perovskite. Phys Rev B. 2018;97:054431.
[26] Liu T, Zhao X, Li J, et al. Enhanced control of self-doping in halide perovskites for improved thermoelectric performance. Nat Commun. 2019;10:5750.
[27] Syono Y, Akimoto S-I, Endoh Y. High pressure synthesis of ilmenite and perovskite type MnVO3 and their magnetic properties. Journal of Physics and Chemistry of Solids. 1971;32:243–249.
[28] Aimi A, Mori D, Hiraki K, et al. High-Pressure Synthesis of A-Site Ordered Double Perovskite CaMnTi2O6 and Ferroelectricity Driven by Coupling of A-Site Ordering and the Second-Order Jahn–Teller Effect. Chemistry of Materials. 2014;26:2601–2608.
[29] Zhang S, Saito T, Mizumaki M, et al. Site-Selective Doping Effect in AMn3V4O12 (A = Na+, Ca2+, and La3+). J Am Chem Soc. 2013;135:6056–6060.
[30] Arévalo-López AM, McNally GM, Attfield JP. Large Magnetization and Frustration Switching of Magnetoresistance in the Double-Perovskite Ferrimagnet Mn2FeReO6. Angewandte Chemie International Edition. 2015;54:12074–12077.
[31] Li M-R, Hodges JP, Retuerto M, et al. Mn2MnReO6: Synthesis and Magnetic Structure Determination of a New Transition-Metal-Only Double Perovskite Canted Antiferromagnet. Chemistry of Materials. 2016;28:3148–3158.
[32] Solana-Madruga E, Alharbi KN, Herz M, et al. Unconventional magnetism in the high pressure 'all transition metal' double perovskite Mn2NiReO6. Chemical Communications. 2020;56:12574–12577.
[33] Li M-R, Stephens PW, Croft M, et al. Mn2(Fe0.8Mo0.2)MoO6: A Double Perovskite with Multiple Transition Metal Sublattice Magnetic Effects. Chemistry of Materials. 2018;30:4508–4514.
[34] Nishibori E, Takata M, Kato K, et al. The large Debye–Scherrer camera installed at SPring-8 BL02B2 for charge density studies. Nucl Instrum Methods Phys Res A. 2001;467–468:1045–1048.
[35] Kawaguchi S, Takemoto M, Osaka K, et al. High-throughput powder diffraction measurement system consisting of multiple MYTHEN detectors at beamline BL02B2 of SPring-8. Review of Scientific Instruments. 2017;88:085111.
[36] Momma K, Izumi F. VESTA: a three-dimensional visualization system for electronic and structural analysis. J Appl Crystallogr. 2008;41:653–658.
[37] Izumi F, Momma K. Three-Dimensional Visualization in Powder Diffraction. Solid State Phenomena. 2007;130:15–20.
[38] Brese NE, O'Keeffe M. Bond-valence parameters for solids. Acta Crystallogr B. 1991;47:192–197.
[39] Belik AA, Liu R, Yamaura K. Dielectric and Spin-Glass Magnetic Properties of the A-Site Columnar-Ordered Quadruple Perovskite Sm2CuMn(MnTi3)O12. Materials. 2022;15:8306.
[40] Dalal B, Kang X, Matsushita Y, et al. Inverse exchange bias effects and magnetoelectric coupling of the half-doped perovskite-type chromites Gd0.5Sr0.5CrO3 and Gd0.5Ca0.5CrO3. Phys Rev B. 2022;106:104425.
[41] Efros AL, Shklovskii BI. Coulomb gap and low temperature conductivity of disordered systems. Journal of Physics C: Solid State Physics. 1975;8:L49–L51.